materials

MDPI

Article

Application of First-Order Shear Deformation Theory on Vibration Analysis of Stepped Functionally Graded Paraboloidal Shell with General Edge Constraints

Fuzhen Pang, Haichao Li *, Fengmei Jing * and Yuan Du

College of Shipbuilding Engineering, Harbin Engineering University, Harbin 150001, China; pangfuzhen@hrbeu.edu.cn (F.P.); duyuan@hrbeu.edu.cn (Y.D.)

* Correspondence: lihaichao@hrbeu.edu.cn (H.L.); jingfengmei@hrbeu.edu.cn (F.J.); Tel.: +86-451-82589161 (H.L.)

Received: 25 November 2018; Accepted: 21 December 2018; Published: 25 December 2018

Abstract: The paper introduces a semi-analytical approach to analyze free vibration characteristics of stepped functionally graded (FG) paraboloidal shell with general edge conditions. The analytical model is established based on multi-segment partitioning strategy and first-order shear deformation theory. The displacement components along axial direction are represented by Jacobi polynomials, and the Fourier series are utilized to express displacement components in circumferential direction. Based on penalty method about spring stiffness technique, the general edge conditions of doubly curved paraboloidal shell can be easily simulated. The solutions about doubly curved paraboloidal shell were solved by approach of Rayleigh–Ritz. Convergence study about boundary parameters, Jacobi parameters et al. are carried out, respectively. The comparison with published literatures, FEM and experiment results show that the present method has good convergence ability and excellent accuracy.

Keywords: stepped FG paraboloidal shell; general edge conditions; spring stiffness technique; free vibration characteristics

1. Introduction

The stepped FG paraboloidal shells are very useful in the engineering. The vibration problems of the structures have always been the concern of the research: Fantuzzi et al. [1] investigated free vibration behavior of FG cylindrical and spherical shells. On the base of FSDT, Tornabene and Reddy [2] used the GDQ approach to investigate the vibration behavior of FGM shells and panels. Based on higher-order finite element method, Pradyumna and Bandyopadhyay [3] studied the vibration behavior of FG structures. Jouneghani et al. [4] also investigated the characteristics of FG doubly curved shells. Chen et al. [5] obtained the vibration characteristics of FG sandwich structure based on shear deformation theory. Wang et al. [6–9] investigated the approach of Improved Fourier to study vibration phenomenon of various structures. Tornabene et al. [10–12] used the GDQ method to research four parameter FG composite structures. Fazzolari and Carrera [13] solved the vibration issues of FG structures based on Ritz minimum energy approach. Kar and Panda [14] studied vibration characteristics of FG spherical shell by FEM. Tornabene [15] focused on the dynamic behavior of FG structures. Zghal [16] investigated the vibration characteristics of FG shells. Kulikov et al. [17] dealt with a recently developed approach to analyze free vibration behavior of FG plates by the formulations of sampling surfaces. Kapuria et al. [18] developed a four-node quadrilateral element method to analyze dynamic vibration of FGM shallow shells.

In field of FG stepped shells, Hosseini-Hashemi et al. [19] proposed an accurate solution to study vibration characteristics of stepped FG plates. Bambill et al. [20] solved vibrations behavior of axially FG beams with stepped changes in geometry. Vinyas and Kattimani [21,22] carried out the static analysis of stepped FG beam and plates with various loads. Su et al. [23] presented an effective method to study free vibration of stepped FG beams.

From literatures reviewed, we can find that many scholars applied Rayleigh Ritz method, GDQ method, Improved Fourier series method, FEM and Haar Wavelet Discretization method etc. to study vibration characteristics of FG doubly curved structures. There are no literatures put attentions on free vibration problems of stepped FG paraboloidal shell. So, it is very important to propose a unified formulation to study free vibration behaviors of stepped FG paraboloidal shell subject to general edge conditions.

2. Fundamental Theory

2.1. The Description of the Model

The model of stepped FG paraboloidal shell is described in Figure 1. h_i represents the thickness of the structure. The stepped structure is obtained by the curve c_1c_2. The model is established on the basis of orthogonal coordinate system (φ, θ, z), which represent axial, circumferential and normal directions, respectively. The displacements are represented by u, v and w, respectively.

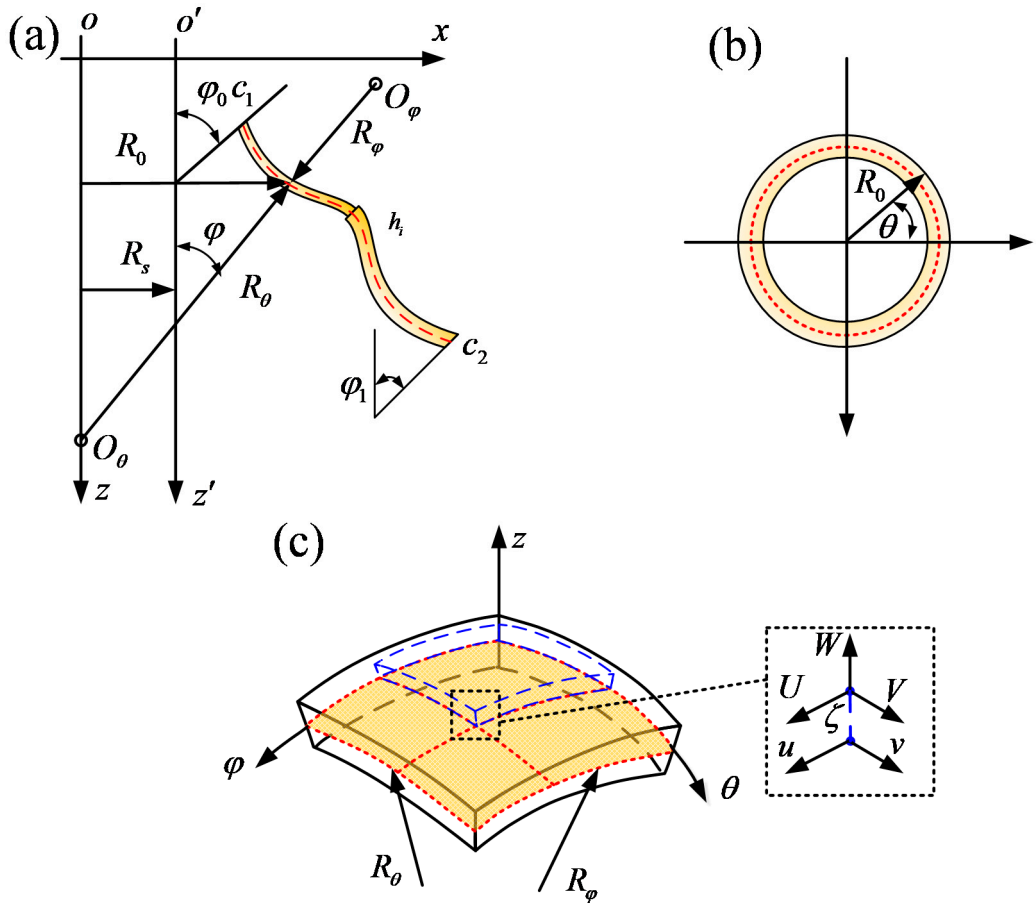

Figure 1. Geometry notations and coordinate system of stepped FG paraboloidal shell. (**a**) Geometric relationship; (**b**) cross-section; (**c**) coordinate system.

The doubly-curved paraboloidal shell is shown in Figure 2. The displacement components of stepped FG paraboloidal shell are represented by U, V and W. In addition, the doubly curved paraboloidal shell is divided into H shell segments along axial direction [24,25].

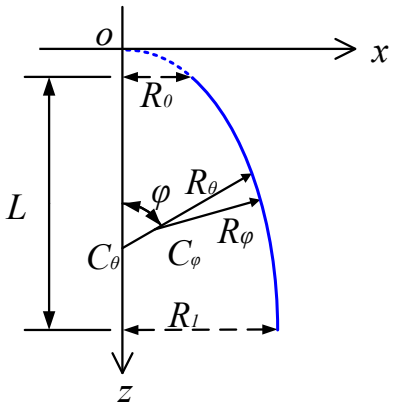

Figure 2. The geometric of doubly curved paraboloidal shell.

The Young's modulus E, Poisson's ratios ν and mass density ρ of two typical FG models are shown as follow [26–32]:

$$E(z) = (E_c - E_m)V_c + E_m \tag{1a}$$

$$\rho(z) = (\rho_c - \rho_m)V_c + \rho_m \tag{1b}$$

$$\nu(z) = (\nu_c - \nu_m)V_c + \nu_m \tag{1c}$$

where c and m denote the ceramic and metallic constituents, respectively. The volume fractions V_c are shown as follow [33]:

$$\mathrm{FGM_I}(a/b/c/p) : V_c = \left[1 - a\left(\frac{1}{2} + \frac{z}{h}\right) + b\left(\frac{1}{2} + \frac{z}{h}\right)^c\right]^p \tag{2a}$$

$$\mathrm{FGM_{II}}(a/b/c/p) : V_c = \left[1 - a\left(\frac{1}{2} - \frac{z}{h}\right) + b\left(\frac{1}{2} - \frac{z}{h}\right)^c\right]^p \tag{2b}$$

where z and p represent the thickness and power law exponent of the structure, respectively. We should note that the value of parameter p takes only positive values. The symbols a, b and c are the key parameters which affect the property of FG material largely. As the volume fraction, the total value of which should be the one. From Equations (1) and (2), we can easily get that the functionally graded material will be the isotropic material when the power law exponent equal to infinity or zero. The variations V_c about various values of a, b, c and p are showed in Figure 3. In addition, we should note that the distributions of volume fraction (2a) and (2b) are mirror reflections. Thus, the Variations V_c of $\mathrm{FGM_{II}}$ are ignored in Figure 3. The detailed descriptions of FG material are reported in Refs. [34–36].

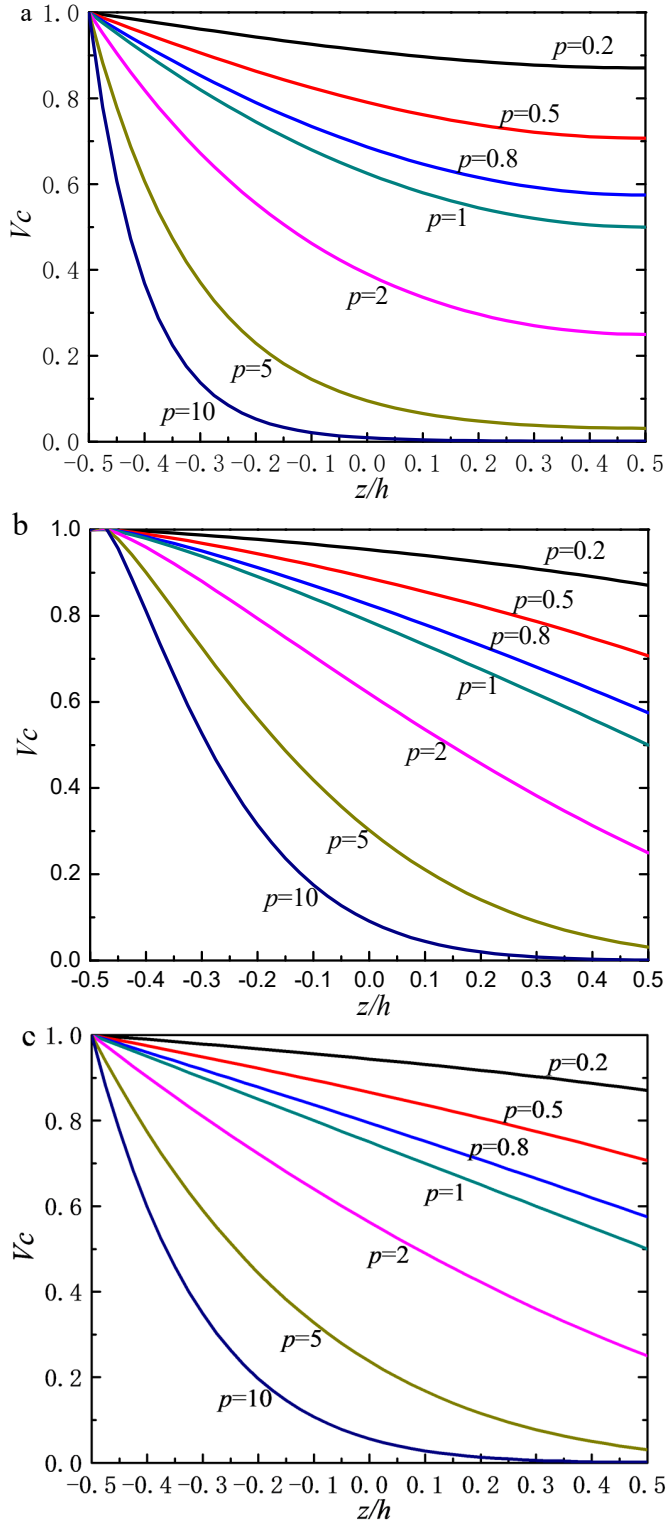

Figure 3. The variations V_c about various values of a, b, c and p: (**a**) FGM_I (a = 0; b = 0.5; c = 2; p); (**b**) FGM_I (a = 1; b = 0.5; c = 0.8; p); (**c**) FGM_I (a = 0; b = −0.5; c = 1; p).

2.2. Energy Equations of Stepped FG Paraboloidal Shell

The displacements of ith segment in stepped FG paraboloidal shell are shown as below:

$$\overline{U}^i(\varphi,\theta,z,t) = u^i(\varphi,\theta,t) + z\psi^i_\varphi(\varphi,\theta,t) \tag{3a}$$

$$\overline{V}^i(\varphi,\theta,z,t) = v^i(\varphi,\theta,t) + z\psi_\theta^i(\varphi,\theta,t) \tag{3b}$$

$$\overline{W}^i(\varphi,\theta,z,t) = w^i(\varphi,\theta,t) \tag{3c}$$

The strains of stepped FG paraboloidal shell are shown as follow

$$\varepsilon_\varphi^i = \varepsilon_\varphi^{0,i} + z\kappa_\varphi^{0,i}\varepsilon_\theta^i = \varepsilon_\theta^{0,i} + z\kappa_\theta^{0,i} \tag{4a}$$

$$\gamma_{\varphi\theta}^i = \gamma_{\varphi\theta}^{0,i} + z\kappa_{\varphi\theta}^{0,i}\gamma_{\varphi z}^i = \gamma_{\varphi z}^{0,i}\gamma_{\theta z}^i = \gamma_{\theta z}^{0,i} \tag{4b}$$

where ε_φ^i, ε_θ^i, $\varepsilon_{\varphi\theta}^i$, $\gamma_{\varphi z}^{0,i}$, $\gamma_{\theta z}^{0,i}$, k_φ^i, k_θ^i and $k_{\varphi\theta}^i$ are given as:

$$\varepsilon_\varphi^{0,i} = \frac{1}{A}\frac{\partial u^i}{\partial\varphi} + \frac{v^i}{AB}\frac{\partial A}{\partial\theta} + \frac{w^i}{R_\varphi} \tag{5a}$$

$$\varepsilon_\theta^{0,i} = \frac{1}{B}\frac{\partial v^i}{\partial\theta} + \frac{u^i}{AB}\frac{\partial B}{\partial\varphi} + \frac{w^i}{R_\theta} \tag{5b}$$

$$\gamma_{\varphi\theta}^{0,i} = \frac{A}{B}\frac{\partial}{\partial\theta}\left(\frac{u^i}{A}\right) + \frac{B}{A}\frac{\partial}{\partial\varphi}\left(\frac{v^i}{B}\right) \tag{5c}$$

$$\kappa_\varphi^i = \frac{1}{A}\frac{\partial\psi_\varphi^i}{\partial\varphi} + \frac{\psi_\theta^i}{AB}\frac{\partial A}{\partial\theta} \tag{5d}$$

$$\kappa_\theta^i = \frac{1}{B}\frac{\partial\psi_\theta^i}{\partial\theta} + \frac{\psi_\varphi^i}{AB}\frac{\partial B}{\partial\varphi} \tag{5e}$$

$$\kappa_{\varphi\theta}^i = \frac{A}{B}\frac{\partial}{\partial\theta}\left(\frac{\psi_\varphi^i}{A}\right) + \frac{B}{A}\frac{\partial}{\partial\varphi}\left(\frac{\psi_\theta^i}{B}\right) \tag{5f}$$

$$\gamma_{\varphi z}^{0,i} = \frac{1}{A}\frac{\partial w^i}{\partial\varphi} - \frac{u^i}{R_\varphi} + \psi_\varphi^i \tag{5g}$$

$$\gamma_{\theta z}^{0,i} = \frac{1}{B}\frac{\partial w^i}{\partial\theta} - \frac{v^i}{R_\theta} + \psi_\theta^i \tag{5h}$$

For doubly curved paraboloidal shell, the symbols A and B are shown as below [37,38]:

$$A = R_\varphi, B = R_\theta\sin\varphi \tag{6}$$

Based on Hooke's law, the stresses corresponding to strains can be expressed as:

$$\begin{Bmatrix} \sigma_\varphi^i \\ \sigma_\theta^i \\ \tau_{\varphi\theta}^i \\ \tau_{\varphi z}^i \\ \tau_{\theta z}^i \end{Bmatrix} = \begin{bmatrix} Q_{11}(z) & Q_{12}(z) & 0 & 0 & 0 \\ Q_{12}(z) & Q_{11}(z) & 0 & 0 & 0 \\ 0 & 0 & Q_{66}(z) & 0 & 0 \\ 0 & 0 & 0 & Q_{66}(z) & 0 \\ 0 & 0 & 0 & 0 & Q_{66}(z) \end{bmatrix} \begin{Bmatrix} \varepsilon_\varphi^i \\ \varepsilon_\theta^i \\ \gamma_{\varphi\theta}^i \\ \gamma_{\varphi z}^i \\ \gamma_{\theta z}^i \end{Bmatrix} \tag{7}$$

where σ_φ^i and σ_θ^i are normal stresses; $\tau_{\varphi\theta}^i$, $\tau_{\varphi z}^i$ and $\tau_{\theta z}^i$ are shear stresses. The $Q_{ij}(z)$ are defined as follows:

$$Q_{11}(z) = \frac{E(z)}{1-\nu^2(z)},\ Q_{12}(z) = \frac{\nu(z)E(z)}{1-\nu^2(z)},\ Q_{66}(z) = \frac{E(z)}{2[1+\nu(z)]} \tag{8}$$

The force and moment resultants can be obtained as follow:

$$\begin{Bmatrix} N_\varphi^i \\ N_\theta^i \\ N_{\varphi\theta}^i \end{Bmatrix} = \begin{bmatrix} A_{11} & A_{12} & 0 \\ A_{12} & A_{22} & 0 \\ 0 & 0 & A_{66} \end{bmatrix} \begin{Bmatrix} \varepsilon_\varphi^{0,i} \\ \varepsilon_\theta^{0,i} \\ \gamma_{\varphi\theta}^{0,i} \end{Bmatrix} + \begin{bmatrix} B_{11} & B_{12} & 0 \\ B_{12} & B_{22} & 0 \\ 0 & 0 & B_{66} \end{bmatrix} \begin{Bmatrix} \varepsilon_\varphi^{0,i} \\ \varepsilon_\theta^{0,i} \\ \gamma_{\varphi\theta}^{0,i} \end{Bmatrix} \tag{9a}$$

$$\begin{Bmatrix} M_\varphi^i \\ M_\theta^i \\ M_{\varphi\theta}^i \end{Bmatrix} = \begin{bmatrix} B_{11} & B_{12} & 0 \\ B_{12} & B_{22} & 0 \\ 0 & 0 & B_{66} \end{bmatrix} \begin{Bmatrix} \varepsilon_\varphi^{0,i} \\ \varepsilon_\theta^{0,i} \\ \gamma_{\varphi\theta}^{0,i} \end{Bmatrix} + \begin{bmatrix} D_{11} & D_{12} & 0 \\ D_{12} & D_{22} & 0 \\ 0 & 0 & D_{66} \end{bmatrix} \begin{Bmatrix} \kappa_\varphi^i \\ \kappa_\theta^i \\ \kappa_{\varphi\theta}^i \end{Bmatrix} \tag{9b}$$

$$\begin{Bmatrix} Q_\varphi^i \\ Q_\theta^i \end{Bmatrix} = \overline{\kappa} \begin{bmatrix} A_{66} & 0 \\ 0 & A_{66} \end{bmatrix} \begin{bmatrix} \gamma_{\varphi z}^{0,i} \\ \gamma_{\theta z}^{0,i} \end{bmatrix} \tag{9c}$$

where $\overline{\kappa}$ is shear correction factor. A_{ij}, B_{ij} and D_{ij} are obtained by following integral:

$$(A_{ij}, B_{ij}, D_{ij}) = \int_{-h/2}^{h/2} Q_{ij}(z)(1, z, z^2)dz \tag{10}$$

The strain energy of the select segment can be expressed from Equation (11) as shown:

$$U^i = \frac{1}{2}\iiint_V \begin{pmatrix} N_\varphi^i \varepsilon_\varphi^{0,i} + N_\theta^i \varepsilon_\theta^{0,i} + N_{\varphi\theta}^i \gamma_{\varphi\theta}^{0,i} + M_\varphi^i k_\varphi^i + \\ M_\theta^i k_\theta^i + M_{\varphi\theta}^i k_{\varphi\theta}^i + Q_\varphi^i \gamma_{\varphi z}^{0,i} + Q_\theta^i \gamma_{\theta z}^{0,i} \end{pmatrix} ABd\varphi d\theta dz \tag{11}$$

To save the space of this paper, the Equation (11) can be expressed as $U^i = U_S^i + U_B^i + U_{BC}^i$. The detailed description of U_S^i, U_B^i and U_{BC}^i are shown in Appendix A.

The maximum kinetic energy of the select segment can be obtained from Equation (12) as shown:

$$\begin{aligned} T^i &= \tfrac{1}{2}\iiint_V \rho(z)\left[\left(\dot{U}^i\right)^2 + \left(\dot{V}^i\right)^2 + \left(\dot{W}^i\right)^2\right]\left(1+\tfrac{z}{R_\varphi}\right)\left(1+\tfrac{z}{R_\theta}\right)ABd\varphi d\theta dz = [\ ] \\ &= \tfrac{1}{2}\int_{\varphi_0}^{\varphi_1}\int_0^{2\pi}\left\{I_0\left[\left(u^i\right)^2 + \left(v^i\right)^2 + \left(w^i\right)^2\right] + 2I_1\left(u^i\psi_\varphi^i + v^i\psi_\theta^i\right) + I_2\left[\left(\psi_\varphi^i\right)^2 + \left(\psi_\theta^i\right)^2\right]\right\}ABd\varphi d\theta \end{aligned} \tag{12}$$

where the dot denotes the differentiation about time, whereas three integrals are defined as follows:

$$(I_0, I_1, I_2) = \int_{-h/2}^{h/2} \rho(z)\left(1+\frac{z}{R_\varphi}\right)\left(1+\frac{z}{R_\theta}\right)\left(1, z, z^2\right)dz \tag{13}$$

The energy in two sides of boundary springs can be expressed as:

$$\begin{aligned} U_b = &\tfrac{1}{2}\int_0^{2\pi}\int_{-h/2}^{h/2}\left\{k_{u,0}u^2 + k_{v,0}v^2 + k_{w,0}w^2 + k_{\varphi,0}\psi_\varphi^2 + k_{\theta,0}\psi_\theta^2\right\}_{\varphi=\varphi_{r,0}} Bd\theta dz \\ &+\tfrac{1}{2}\int_0^{2\pi}\int_{-h/2}^{h/2}\left\{k_{u,1}u^2 + k_{v,1}v^2 + k_{w,1}w^2 + k_{\varphi,1}\psi_\varphi^2 + k_{\theta,1}\psi_\theta^2\right\}_{\varphi=\varphi_{r,1}} Bd\theta dz \end{aligned} \tag{14}$$

where $k_{t,0}$ $(t = u, v, w, \varphi, \theta)$ and $k_{t,1}$ denote the value of springs at two sides.

The energy in connective springs of two neighbor segments is expressed as:

$$U_s^i = \frac{1}{2}\int_0^{2\pi}\int_{-h/2}^{h/2}\left\{\begin{array}{l} k_u\left(u^i - u^{i+1}\right)^2 + k_v\left(v^i - v^{i+1}\right)^2 + k_w\left(w^i - w^{i+1}\right)^2 \\ +k_\varphi\left(\psi_\varphi^i - \psi_\varphi^{i+1}\right)^2 + k_\theta\left(\psi_\theta^i - \psi_\theta^{i+1}\right)^2 \end{array}\right\}_{i,i+1} Bd\theta dz \tag{15}$$

The total energy of the constraint conditions can be expressed as:

$$U_{BC} = U_b + \sum_{i=1}^{H-1} U_s^i \tag{16}$$

2.3. Displacement Functions and Solution

Proper selection of the admissible displacement function is a critical factor for the accuracy of final solution [39–43]. As displayed in literatures [44,45], classical Jacobi polynomials are valued in range of $\phi \in [-1, 1]$. Typical Jacobi polynomials $P_i^{(\alpha,\beta)}(\phi)$ of degree i are shown as below in present method.

$$P_0^{(\alpha,\beta)}(\phi) = 1 \tag{17a}$$

$$P_1^{(\alpha,\beta)}(\phi) = \frac{\alpha+\beta+2}{2}\phi - \frac{\alpha-\beta}{2} \tag{17b}$$

$$\begin{aligned} P_i^{(\alpha,\beta)}(\phi) = {} & \frac{(\alpha+\beta+2i-1)\{\alpha^2-\beta^2+\phi(\alpha+\beta+2i)(\alpha+\beta+2i-2)\}}{2i(\alpha+\beta+i)(\alpha+\beta+2i-2)} P_{i-1}^{(\alpha,\beta)}(\phi) \\ & - \frac{(\alpha+i-1)(\beta+i-1)(\alpha+\beta+2i)}{i(\alpha+\beta+i)(\alpha+\beta+2i-2)} P_{i-2}^{(\alpha,\beta)}(\phi) \end{aligned} \tag{17c}$$

where $\alpha, \beta > -1$ and $i = 2, 3, \ldots$

Thus, the displacement functions of shell segments can be written in form of Equation (18) as shown:

$$u = \sum_{m=0}^{M} U_m P_m^{(\alpha,\beta)}(\phi)\cos(n\theta)e^{i\omega t} \tag{18a}$$

$$v = \sum_{m=0}^{M} V_m P_m^{(\alpha,\beta)}(\phi)\sin(n\theta)e^{i\omega t} \tag{18b}$$

$$w = \sum_{m=0}^{M} W_m P_m^{(\alpha,\beta)}(\phi)\cos(n\theta)e^{i\omega t} \tag{18c}$$

$$\psi_\varphi = \sum_{m=0}^{M} \psi_{\varphi m} P_m^{(\alpha,\beta)}(\phi)\cos(n\theta)e^{i\omega t} \tag{18d}$$

$$\psi_\theta = \sum_{m=0}^{M} \psi_{\theta m} P_m^{(\alpha,\beta)}(\phi)\cos(n\theta)e^{i\omega t} \tag{18e}$$

where U_m, V_m, W_m, $\psi_{\varphi m}$ and $\psi_{\theta m}$ are unknown coefficients. n and m denote the semi wave number in axial and circumferential direction, respectively. M is highest degrees of semi wave number m. The total Lagrangian energy functions L can be obtained as it is shown in Equation (19):

$$L = \sum_{i=1}^{H}\left(T^i - U^i\right) - U_{BC} \tag{19}$$

The total Lagrangian energy function L is shown in Equation (20):

$$\frac{\partial L}{\partial \vartheta} = 0 \quad \vartheta = U_m, V_m, W_m, \psi_{\varphi m}, \psi_{\theta m} \tag{20}$$

Substituting Equations (11), (12), (16), (18), (19) into Equation (20), then Equation (21) can be obtained as:

$$\left(\mathbf{K} - \omega^2\mathbf{M}\right)\mathbf{Q} = 0 \tag{21}$$

where $\mathbf{K}$ and $\mathbf{M}$ denote stiffness and mass matrixes, respectively. $\mathbf{Q}$ is unknown coefficient matrix.

3. Analysis of Examples

The general boundary conditions are denoted by the abbreviations. Thus the abbreviations F, C, SD, SS and Ei respectively represent free, clamped, shear diaphragm, shear support and elastic boundary conditions. The material properties are chosen as: $E_m = 70$ GPa, $E_c = 168$ GPa, $\rho_c = 5700$ kg/m^3, $\rho_m = 2707$ kg/m^3, $\nu_m = \nu_c = 0.3$, $M = 8$, $\alpha = 0$, $\beta = -0.5$, $H = 5$. The geometrical dimensions are chosen as follows: $R_0 = 0.2$ m, $R_1 = 1$ m, $L_p = 1$ m, h_1:h_2:h_3:h_4:h_5 = 0.04:0.045:0.05:0.055:0.06 . The results of this paper are handle by: $\Omega = \omega R_1 \sqrt{\rho_c / E_c}$.

3.1. Convergence Analysis

Figure 4 shows the frequency parameter of stepped FGM$_\mathrm{I}$ ($a = 1$; $b = -0.5$; $c = 2$; $p = 2$) doubly curved paraboloidal shell with different boundary parameters. We can get that the spring stiffness values in range of 10–10^{10} E_c can converge to stable, regardless of the kinds of spring. In other words, for clamped boundary condition, the spring stiffness can be assigned within the range of 10–10^{10} E_c. Based on the boundary parameters analysis, the general edge constraints are be provided as shown Table 1.

Table 1. Spring stiffness values.

BC	$k_{u,0}$, $k_{u,1}$	$k_{v,0}$, $k_{v,1}$	$k_{w,0}$, $k_{w,1}$	$k_{\varphi,0}$, $k_{\varphi,1}$	$k_{\theta,0}$, $k_{\theta,1}$
F	0	0	0	0	0
SD	0	10^3 E_c	10^3 E_c	0	0
SS	10^3 E_c	10^3 E_c	10^3 E_c	0	10^3 E_c
C	10^3 E_c	10^3 E_c	10^3 E_c	10^3 E_c	10^3 E_c
E1	10^{-3} E_c	10^3 E_c	10^3 E_c	10^3 E_c	10^3 E_c
E2	10^3 E_c	10^{-3} E_c	10^3 E_c	10^3 E_c	10^3 E_c
E3	10^{-3} E_c	10^{-3} E_c	10^3 E_c	10^3 E_c	10^3 E_c

The relative percentage errors of stepped FGM$_\mathrm{I}$ ($a = 1$; $b = -0.5$; $c = 2$; $p = 2$) paraboloidal shell with various Jacobi parameters are presented in Figure 5. The results of $\alpha = \beta = 0$ are selected as the reference values. We can easily conclude from Figure 5 that different Jacobi parameters will lead to almost the same results when n is a fixed value. The maximum relative error is less than 8×10^{-8}. Thus, we can conclude that displacement functions consisting with Jacobi polynomial and Fourier series are perfectly appropriate. The most advantages of proposed method are the unified Jacobi polynomials, which make the displacement functions easier to select in contrast with other approaches. Figure 6 exhibits the results of stepped FG paraboloidal shell about truncation. We can get that the convergent results can be guaranteed when M is higher than 5. M is defined as the value of eight in this paper.

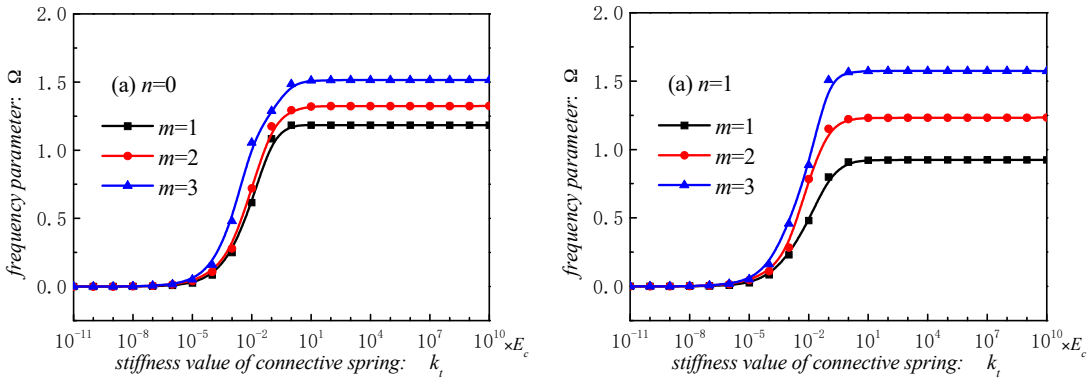

Figure 4. *Cont.*

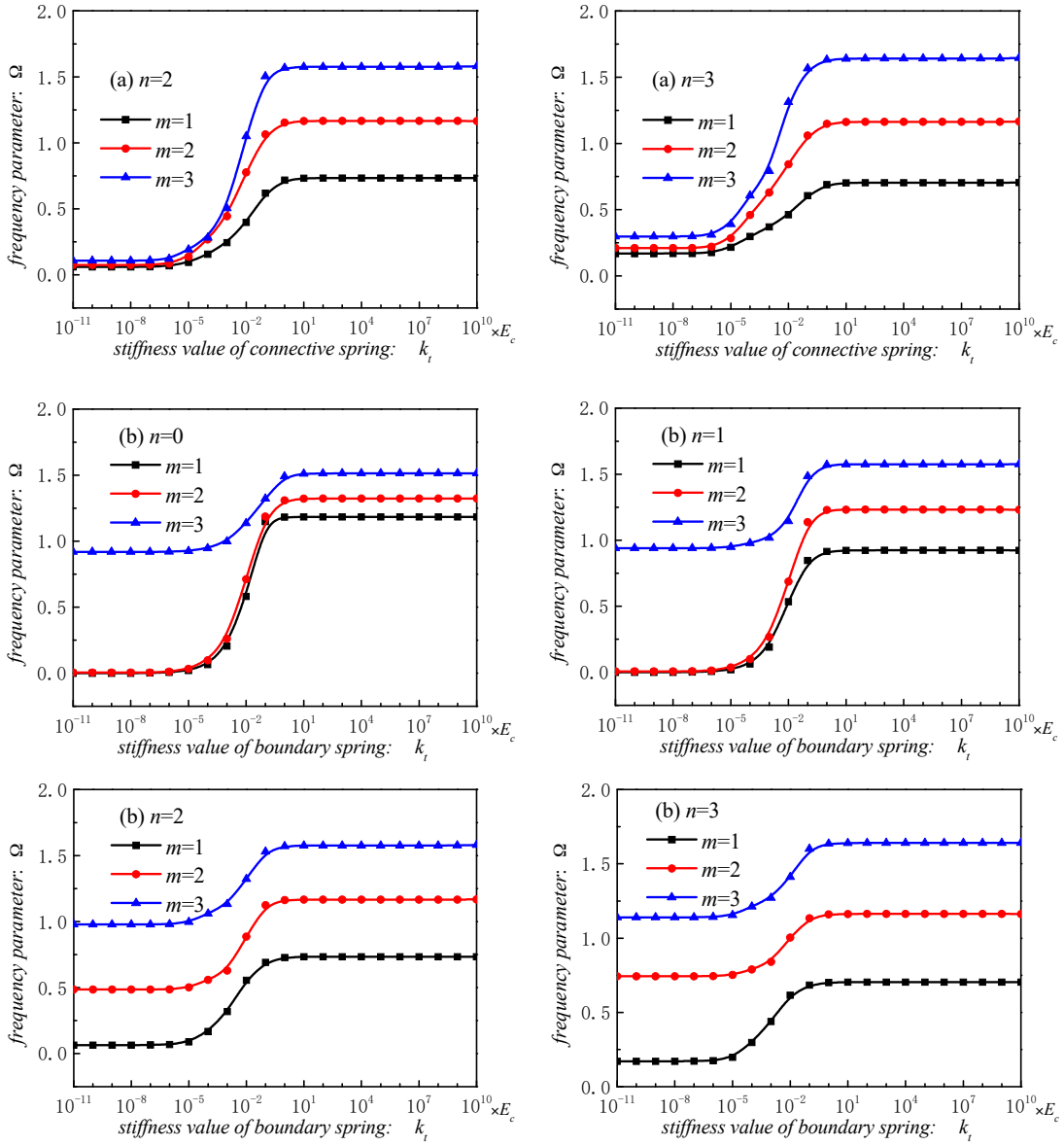

Figure 4. Frequency parameters Ω of stepped FG paraboloidal shell with various boundary parameters.

Table 2 exhibits the frequency parameter Ω of FGM_I (a = 1; b = 0; c; p) about the value of H, and the verification model is a spherical shell. The results are compared with those in literature [46]. From Table 2, we can conclude that the results will converge quickly as the value of H increase. We can also conclude that very high value of M is unnecessary. In addition, it can be obtained from Table 2 that the present method is strongly agreed with reference data.

Table 2. Frequency parameter Ω of the FGM_I (a = 1; b = 0; c; p) spherical shell structure (BC; C–C, m = 1).

Power-Law Exponent	Number of the Segment (H_e)								Ref [46]
	n	**2**	**3**	**4**	**5**	**6**	**7**	**8**	
p = 0.6	1	1.0569	1.0569	1.0568	1.0568	1.0568	1.0568	1.0568	1.0538
	2	1.0379	1.0376	1.0374	1.0372	1.0371	1.0371	1.0370	1.0354
	3	1.0319	1.0317	1.0314	1.0312	1.0312	1.0310	1.0310	1.0294
	4	1.0760	1.0757	1.0755	1.0752	1.0751	1.0750	1.0749	1.0733
	5	1.1588	1.1586	1.1584	1.1581	1.1581	1.1580	1.1580	1.1559

Table 2. *Cont.*

Power-Law Exponent	Number of the Segment (H_e)								Ref [46]
	n	**2**	**3**	**4**	**5**	**6**	**7**	**8**	
$p = 5$	1	1.0446	1.0446	1.0446	1.0445	1.0445	1.0445	1.0445	1.0411
	2	1.0116	1.0115	1.0113	1.0111	1.0110	1.0109	1.0108	1.0085
	3	1.0085	1.0083	1.0082	1.0080	1.0079	1.0079	1.0078	1.0053
	4	1.0572	1.0571	1.0569	1.0568	1.0566	1.0565	1.0563	1.0539
	5	1.1470	1.1468	1.1467	1.1465	1.1464	1.1464	1.1463	1.1433
$p = 20$	1	1.0282	1.0282	1.0281	1.0281	1.0281	1.0281	1.0281	1.0266
	2	0.9958	0.9957	0.9956	0.9954	0.9953	0.9953	0.9952	0.9945
	3	0.9927	0.9926	0.9924	0.9923	0.9922	0.9921	0.9920	0.9913
	4	1.0407	1.0405	1.0404	1.0403	1.0403	1.0402	1.0399	1.0392
	5	1.1290	1.1289	1.1287	1.1286	1.1285	1.1284	1.1284	1.1273

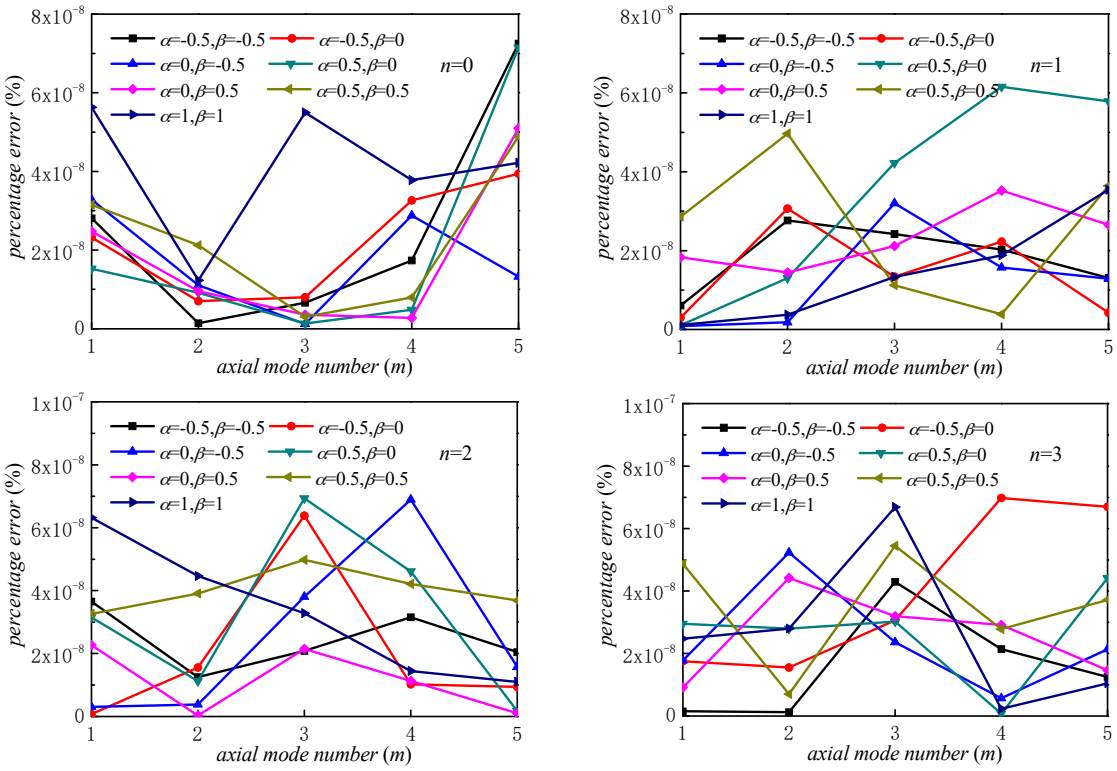

Figure 5. Relative error of frequency parameters Ω in stepped FG paraboloidal shell (BC: C–C).

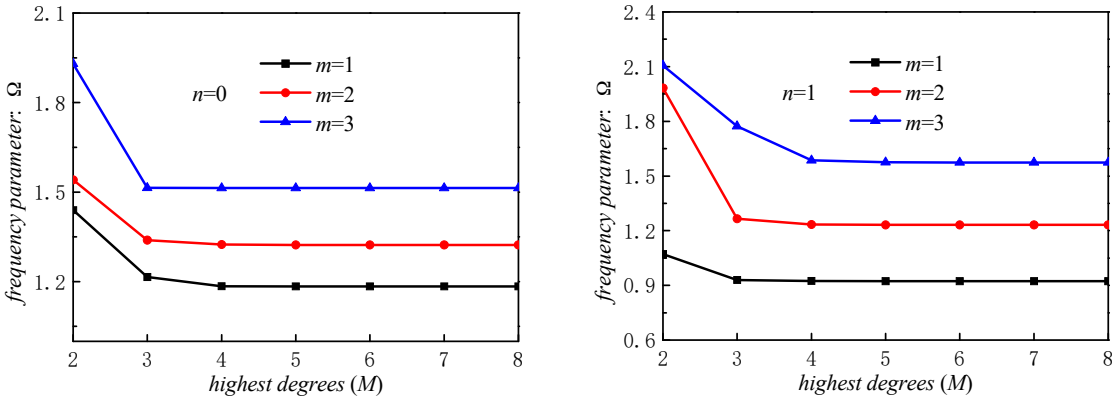

Figure 6. *Cont.*

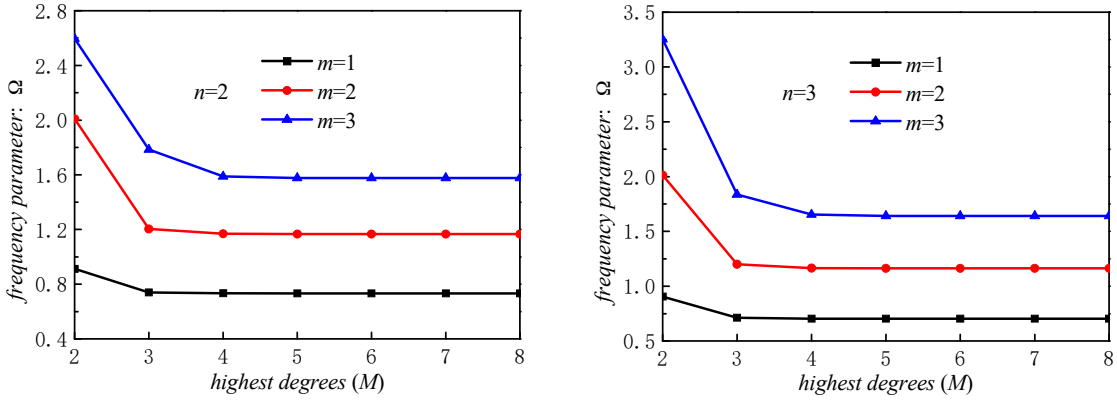

Figure 6. Frequency parameters Ω for various truncation in stepped FG paraboloidal shell.

3.2. Free vibration Behavior of Stepped FG Paraboloidal Shell

Table 3 shows the precision of the approach in solving free vibration behavior of stepped FG paraboloidal shell with clamed boundary condition, and all the FEM commercial program ABAQUS (S4R model) results have converged to stable when the element size is chosen as 0.03 m. In addition, it should be note that the homogeneous elements not graded elements [47] were used in this paper. From the comparison study, we can conclude that the present method is capable to analyze the vibration behaviors of stepped doubly curved paraboloidal shell with general boundary conditions.

Table 3. Comparison of frequency parameter Ω for stepped doubly curved paraboloidal shell (FGM_I (a, b, c, p = 0)).

n	*m*	Proposed Method	FEM
0	1	1.2139	1.2144
	2	1.3579	1.3586
	3	1.5621	1.5645
	4	1.6154	1.6183
1	1	0.9499	0.9504
	2	1.2605	1.2615
	3	1.6030	1.6070
	4	1.9770	1.9725
2	1	0.7521	0.7524
	2	1.1907	1.1924
	3	1.6002	1.6056
	4	2.1071	2.1083
3	1	0.7171	0.7176
	2	1.1811	1.1835
	3	1.6590	1.6566
	4	2.2217	2.2251

To further prove the effectiveness of this method, the experiment test focused on free vibration of cylindrical shell was carried out. It should be note that the cylindrical shell is isotropic. The material properties and geometrical parameters are chosen as: E = 210 GPa, ρ = 7850 kg/m^3, ν = 0.3, R = 0.06 m, L = 0.3 m, h = 0.005 m. The boundary condition is free for isotropic cylindrical shell due to the of the restraints test environment. Figure 7 shows the test instrument and model. In experiment, the hammer was used to strike different positions of cylindrical shells in turn, and acceleration sensors with sensitivity of 100 mv/g were used to collect the vibration response at the same point. Then the time domain signals obtained by test were transformed into frequency domain signals by Fourier transform. The final results of frequencies are shown in Table 4. For natural frequencies obtained by FEM commercial program ABAQUS (S4R model), it is obvious that the structure and material

parameters are the same as the experiment, and it should be note that the results have converge to stable when the mesh size is 0.03 m. From Table 4, it is easy to find that the present results closely agreed with experiment and FEM. For selected five modes, the maximum error of present method and experiment is 2.35%, and the maximum error of present method and FEM is 0.38%. The reason for the large error of present method with the test results are mainly the influence of elastic hoisting boundary and random error. The mode shapes obtained by three different methods are presented in Figure 8.

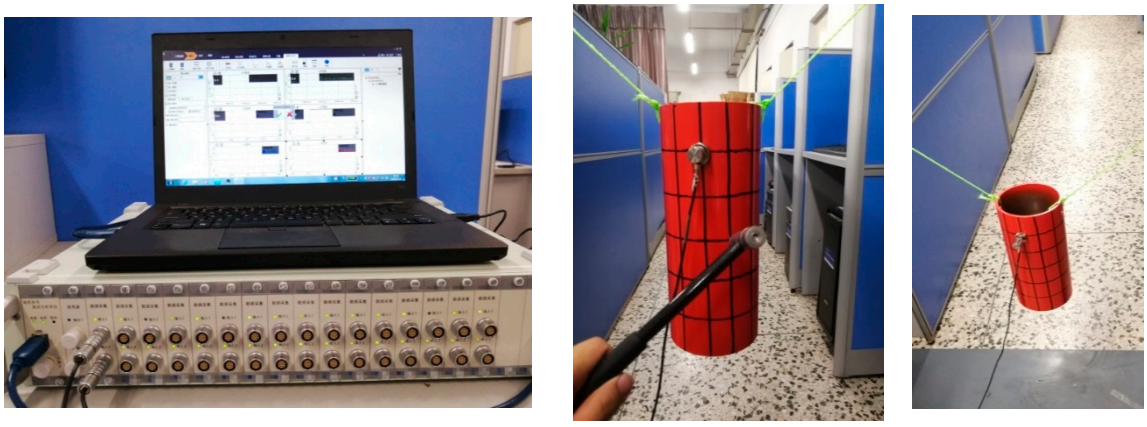

(**a**) (**b**)

Figure 7. Testing instruments and model. (**a**) The test system; (**b**) the test model.

Table 4. Comparison study of the frequencies for cylindrical shell.

n, *m*	Present	Experimental	Error (%)	FEM	Error (%)
0, 1	545.89	551.97	1.11	547.49	0.29
2, 2	582.13	588.39	1.08	581.98	0.03
0, 3	1561.93	1572.53	0.68	1567.90	0.38
2, 3	1618.37	1656.42	2.35	1613.70	0.29
3, 3	2143.98	2169.05	1.17	2150.70	0.31

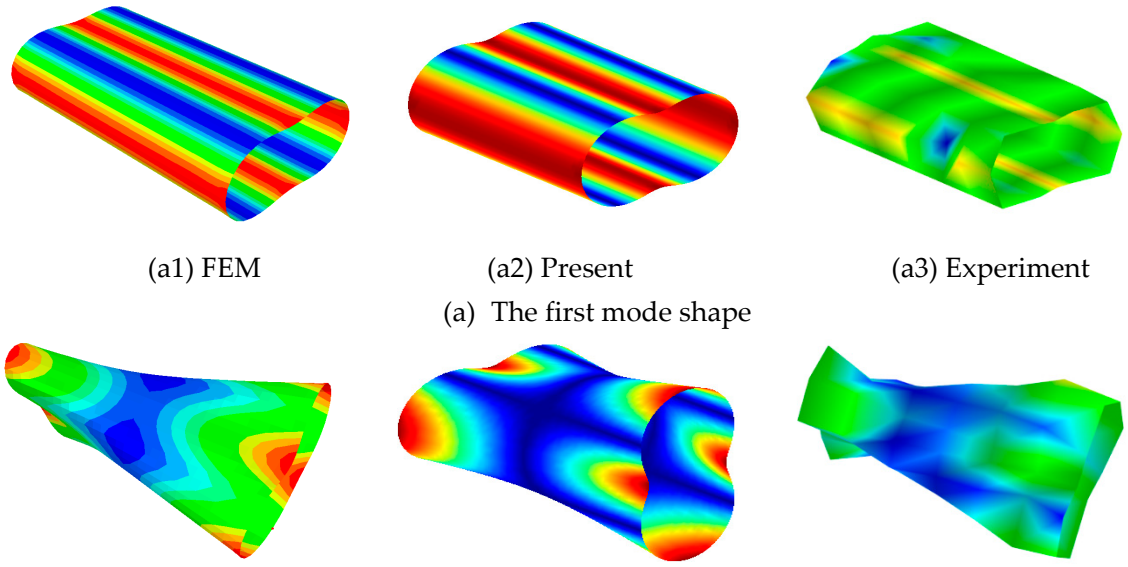

(a1) FEM (a2) Present (a3) Experiment

(a) The first mode shape

(b1) FEM (b2) Present (b3) Experiment

(b) The second mode shape

Figure 8. The selected mode shapes of three kinds of method.

Table 5 exhibits the results of free vibration behaviors for stepped FG paraboloidal shell with various boundary conditions. From Table 5, it is easy to find that the free vibration characteristics are not only influence by boundary conditions, but material parameters. To better reveal the vibration characteristics of the shell, some mode shapes are given in Figure 9.

Table 5. Frequency parameters Ω of stepped paraboloidal shell.

Type	*n*	*m*	Boundary Restraints									
			F–C	**C–C**	**SD–SD**	**SS–SS**	**E1–E1**	**E2–E2**	**E3–E3**	**F–E1**	**F–E2**	**F–SS**
FGM_I (a = 1; b = −0.5; c = 2; p = 2)	1	1	0.7470	0.9238	0.6151	0.8886	0.6736	0.5307	0.2076	0.2171	0.4519	0.7301
		2	1.1767	1.2318	0.8874	1.1522	0.9171	1.2104	0.5468	0.8334	1.1066	1.0967
		3	1.4199	1.5746	1.1503	1.4582	1.2343	1.4709	1.1710	1.1866	1.4113	1.3661
		4	1.6262	1.9378	1.4683	1.8208	1.5746	1.7016	1.4638	1.4535	1.4271	1.6000
		5	1.7717	2.0975	1.8376	2.0156	2.0259	1.9062	1.5645	1.7696	1.7209	1.6947
	2	1	0.5453	0.7334	0.6855	0.6973	0.7196	0.6154	0.5819	0.4742	0.4983	0.5329
		2	0.9432	1.1666	1.0460	1.0800	1.1426	1.1078	0.9250	0.9212	0.8446	0.8894
		3	1.3195	1.5767	1.3190	1.4539	1.3368	1.5389	1.3106	1.3023	1.3013	1.2305
		4	1.7651	2.0848	1.4434	1.9063	1.5690	2.0412	1.4790	1.3588	1.7237	1.6529
		5	2.2154	2.5207	1.8933	2.4718	2.0823	2.2287	1.9788	1.7737	2.1426	2.1436
	3	1	0.6918	0.7037	0.6469	0.6597	0.6939	0.6630	0.6588	0.6816	0.6549	0.6516
		2	1.1043	1.1629	1.0674	1.0763	1.1594	1.1255	1.0998	1.1029	1.0725	1.0362
		3	1.4964	1.6405	1.5063	1.5173	1.6362	1.6151	1.5855	1.4963	1.4798	1.4098
		4	1.9638	2.2032	1.9827	2.0370	2.0021	2.1782	1.8904	1.9536	1.9463	1.8532
		5	2.5376	2.8897	2.0261	2.6731	2.1986	2.8331	2.1627	2.0105	2.5267	2.4127
FGM_{II} (a = 1; b = −0.5; c = 2; p = 2)	1	1	0.7418	0.9171	0.6086	0.8875	0.6689	0.5274	0.2064	0.2161	0.4491	0.7153
		2	1.1663	1.2205	0.8821	1.1388	0.9110	1.1991	0.5427	0.8263	1.0974	1.1007
		3	1.4059	1.5589	1.1408	1.4569	1.2232	1.4590	1.1604	1.1759	1.4010	1.3328
		4	1.6117	1.9209	1.4556	1.7561	1.5588	1.6896	1.4532	1.4381	1.4141	1.6112
		5	1.7523	2.0820	1.8189	2.0554	2.0045	1.8919	1.5520	1.7494	1.7022	1.6794
	2	1	0.5378	0.7271	0.6821	0.6895	0.7136	0.6103	0.5768	0.4670	0.4920	0.5171
		2	0.9331	1.1553	1.0399	1.0802	1.1315	1.0968	0.9159	0.9117	0.8351	0.8909
		3	1.3062	1.5593	1.3101	1.4468	1.3285	1.5218	1.3017	1.2916	1.2878	1.2172
		4	1.7468	2.0615	1.4329	1.8881	1.5518	2.0196	1.4630	1.3468	1.7066	1.6445
		5	2.1931	2.5059	1.8788	2.4820	2.0593	2.2170	1.9600	1.7554	2.1281	2.0916
	3	1	0.6846	0.6968	0.6436	0.6477	0.6872	0.6566	0.6524	0.6746	0.6482	0.6389
		2	1.0906	1.1506	1.0609	1.0731	1.1471	1.1136	1.0877	1.0892	1.0592	1.0300
		3	1.4762	1.6214	1.4944	1.5073	1.6171	1.5961	1.5665	1.4761	1.4597	1.3933
		4	1.9404	2.1772	1.9727	2.0216	1.9913	2.1526	1.8796	1.9316	1.9231	1.8339
		5	2.5057	2.8601	2.0097	2.6553	2.1728	2.8113	2.1386	1.9983	2.4952	2.3801

Table 6 shows the results of stepped FG paraboloidal shell with different power-law exponents, in which four values are included. From Table 6, we can get that the boundary conditions and power-law exponents all will have important impact on the results of the structure.

Table 7 shows the results of stepped FG paraboloidal shell with different thickness distributions. Four kinds of thickness distributions, i.e., h_1:h_2:h_3:h_4:h_5 = 0.04:0.045:0.05:0.055:0.06 are included. It is obvious that the thickness distributions affect the vibration behavior of stepped FG paraboloidal shell largely.

Figures 10–12 exhibit the frequency parameters Ω of stepped FG paraboloidal shell with various parameters a, b, c and p. From selected data, it could be found that a, b and c have a great deal of impact on the results of Ω. In addition, for parameters a and c, the smaller value will obtain the larger results. Figure 13 exhibits the results of stepped FG paraboloidal shell with various stiffness ratios and parameter p. It can be seen that no matter what value of parameter p, the vibration characteristics will decrease with E_c/E_m increasing.

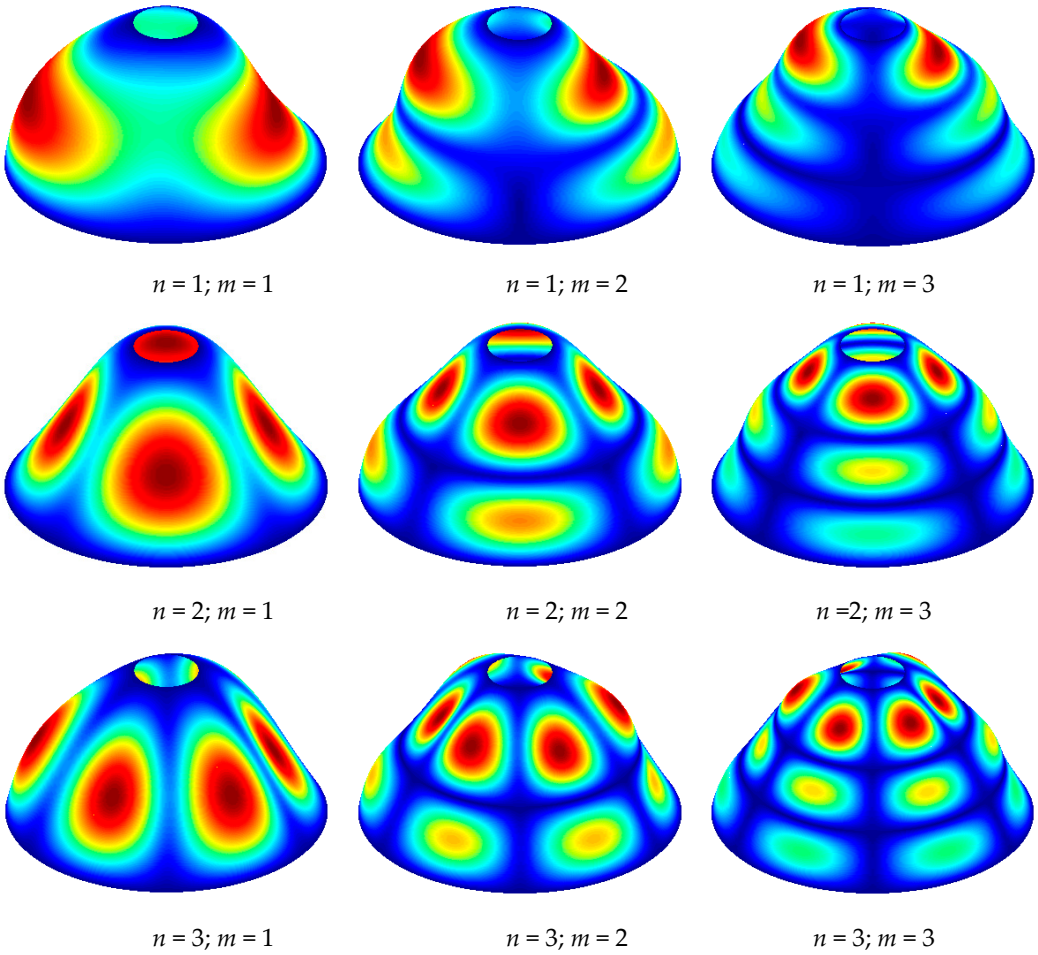

Figure 9. Mode shapes of stepped FG paraboloidal shell (BC: SS–SS).

Table 6. Frequency parameters Ω for stepped FGM_I (a = 1; b = 0.5; c = 2; p) shell with different power-law exponents.

Power-Law Exponents	*n*	*m*	C–C	SD–SD	F–SS
p = 0.2	1	1	0.9480	0.6315	0.7461
		2	1.2583	0.9133	1.1301
		3	1.6007	1.1769	1.3859
	2	1	0.7507	0.7047	0.5374
		2	1.1888	1.0703	0.9119
		3	1.5983	1.3557	1.2499
	3	1	0.7161	0.6612	0.6606
		2	1.1796	1.0868	1.0534
		3	1.6574	1.5264	1.4231
p = 0.5	1	1	0.9451	0.6297	0.7444
		2	1.2550	0.9104	1.1259
		3	1.5971	1.1737	1.3836
	2	1	0.7486	0.7025	0.5369
		2	1.1859	1.0673	0.9090
		3	1.5951	1.3514	1.2472
	3	1	0.7144	0.6593	0.6595
		2	1.1772	1.0841	1.0508
		3	1.6545	1.5232	1.4207

Table 6. *Cont.*

Power-Law Exponents	*n*	*m*	C–C	SD–SD	F–SS
$p = 2$	1	1	0.9321	0.6210	0.7359
		2	1.2395	0.8969	1.1078
		3	1.5796	1.1585	1.3711
	2	1	0.7389	0.6922	0.5332
		2	1.1721	1.0532	0.8959
		3	1.5789	1.3322	1.2339
	3	1	0.7064	0.6508	0.6534
		2	1.1650	1.0712	1.0389
		3	1.6394	1.5074	1.4081
$p = 5$	1	1	0.9164	0.6103	0.7236
		2	1.2221	0.8807	1.0892
		3	1.5625	1.1413	1.3542
	2	1	0.7276	0.6803	0.5280
		2	1.1575	1.0383	0.8832
		3	1.5646	1.3084	1.2210
	3	1	0.6983	0.6422	0.6460
		2	1.1540	1.0597	1.0285
		3	1.6282	1.4954	1.3991

Table 7. Frequency parameters Ω for stepped FGM_I ($a = 1$; $b = 0.5$; $c = 2$; $p = 2$) shell with different thickness distributions.

h_1:h_2:h_3:h_4:h_5	*n*	*m*	C–C	SD–SD	F–SS
0.04:0.05:0.06:0.07:0.08	1	1	0.9579	0.5884	0.7655
		2	1.3085	0.9008	1.1470
		3	1.6903	1.2140	1.4461
	2	1	0.7667	0.6952	0.5476
		2	1.2454	1.1009	0.9267
		3	1.7064	1.2969	1.3145
	3	1	0.7590	0.6841	0.6925
		2	1.2600	1.1513	1.1067
		3	1.7917	1.6410	1.5140
0.08:0.07:0.06:0.05:0.04	1	1	0.8600	0.6915	0.6176
		2	1.1979	0.9477	1.0841
		3	1.6283	1.1045	1.2400
	2	1	0.7026	0.6680	0.5916
		2	1.1782	1.0529	0.9674
		3	1.6697	1.4977	1.3075
	3	1	0.6992	0.6584	0.6578
		2	1.2297	1.1176	1.1192
		3	1.8009	1.6410	1.6103
0.04:0.06:0.08:0.07:0.05	1	1	0.8483	0.5982	0.6988
		2	1.2766	0.8162	1.1448
		3	1.6965	1.1861	1.3817
	2	1	0.6747	0.6343	0.5059
		2	1.2266	1.0603	0.9036
		3	1.7104	1.4039	1.2943
	3	1	0.6993	0.6493	0.6457
		2	1.2530	1.1403	1.1109
		3	1.8046	1.6523	1.5196

Table 7. *Cont.*

h_1:h_2:h_3:h_4:h_5	n	m	C–C	SD–SD	F–SS
0.07:0.05:0.04:0.06:0.08	1	1	1.0086	0.6664	0.7052
		2	1.2356	0.9912	1.0789
		3	1.6421	1.1382	1.4098
	2	1	0.8278	0.7647	0.6457
		2	1.1948	1.0710	0.9595
		3	1.6748	1.2893	1.3483
	3	1	0.8000	0.7185	0.7324
		2	1.2351	1.1212	1.1102
		3	1.7878	1.6336	1.5970

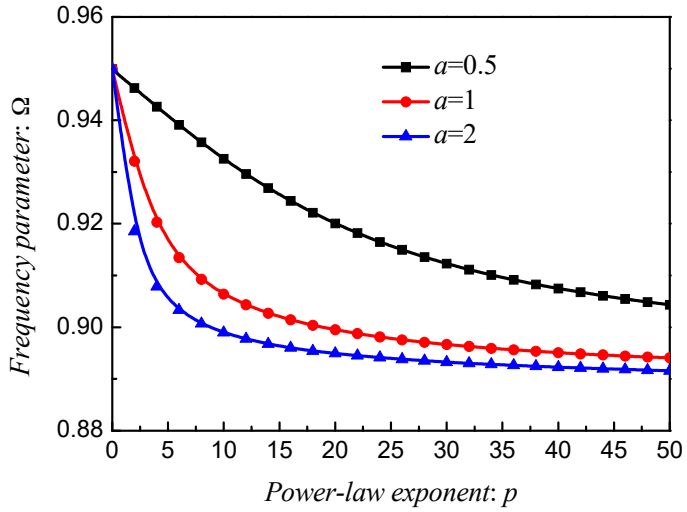

Figure 10. Results about different p and a of stepped FGM_I (a, b = 0.5; c = 2; p) paraboloidal shell.

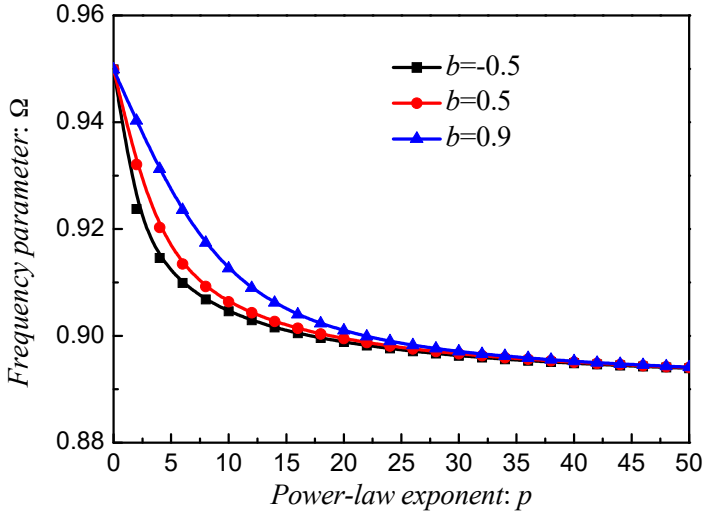

Figure 11. Results about different p and b of stepped FGM_I (a = 1; b, c = 2; p) paraboloidal shell.

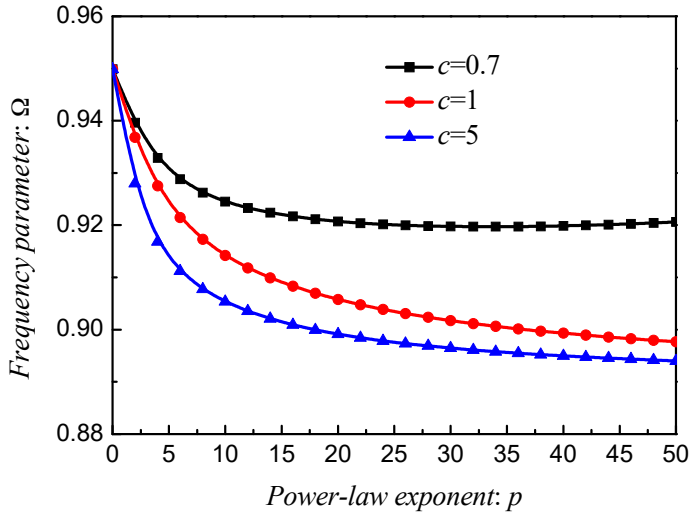

Figure 12. Results about different p and c of stepped FGM_I (a = 1; b = 0.5; c; p) paraboloidal shell.

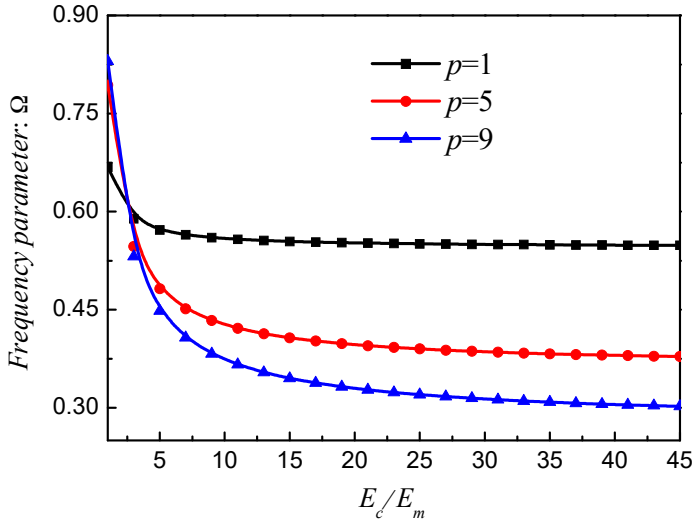

Figure 13. Results about different E_c/E_m and p of stepped FGM_I (a = 1; b = 0.5; c = 2; p) paraboloidal shell.

4. Conclusions

The paper proposed a solving formulation to investigate the free vibration behaviors of stepped FG paraboloidal shell with general boundary conditions. The paper is based on multi-segment strategy and FSDT. The displacement functions are simulated by Jacobi polynomials and Fourier series. To obtain the general boundary conditions of stepped FG paraboloidal shell, the penalty method was adopted. The final modes solutions about FG paraboloidal shell were obtained by Rayleigh–Ritz method. The most discoveries of proposed method are unified Jacobi polynomials, which make the displacement functions easier to select. For convergence analysis, the influence of boundary parameters, numbers of shell segments etc. are examined. The accuracy of this method was verified by the comparison study with those obtained by published literature, FEM, and the experiment. The results of this paper can provide the reference data for future research.

Author Contributions: Conceptualization, F.P. and H.L.; Data curation, H.L. and F.X.; Formal analysis, H.L.; Funding acquisition, F.P.; Investigation, H.L.; Project administration, H.L. and Y.D.

Funding: This study was funded by Naval pre-research project, Ph.D. Student Research and Innovation Fund of the Fundamental Research Funds for the Central Universities (HEUGIP201801), Major innovation projects Of High Technology Ship Funds of Ministry of Industry and Information of China, High Technology Ship Funds of Ministry

of Industry and Information of China, National key Research and Development program (2016YFC0303406), Assembly Advanced Research Fund Of China (6140210020105).

Conflicts of Interest: The authors declare that there is no conflict of interest regarding the publication of this paper.

Appendix A

$$\mathbf{M} = diag\left[\mathbf{M}^1, \mathbf{M}^2, \cdots, \mathbf{M}^H\right] \tag{A1}$$

$$\mathbf{M}^i = \int_{\varphi_i}^{\varphi_{i+1}} \int_0^{2\pi} \begin{bmatrix} M_{uu} & 0 & 0 & M_{u\varphi} & 0 \\ 0 & M_{vv} & 0 & 0 & M_{v\theta} \\ 0 & 0 & M_{ww} & 0 & 0 \\ M_{u\varphi} & 0 & 0 & M_{\varphi\varphi} & 0 \\ 0 & M_{v\theta} & 0 & 0 & M_{\theta\theta} \end{bmatrix} ABd\varphi d\theta \tag{A2}$$

$$\mathbf{M}_{uu} = I_0\mathbf{U}^T\mathbf{U},\ \mathbf{M}_{vv} = I_0\mathbf{V}^T\mathbf{V}, \mathbf{M}_{ww} = I_0\mathbf{W}^T\mathbf{W}, \mathbf{M}_{\varphi\varphi} = I_2\mathbf{\Phi}^T\mathbf{\Phi} \tag{A3}$$

$$\mathbf{M}_{\theta\theta} = I_2\mathbf{\Theta}^T\mathbf{\Theta}, \mathbf{M}_{u\varphi} = I_1\mathbf{U}^T\mathbf{\Phi}, \mathbf{M}_{v\theta} = I_1\mathbf{V}^T\mathbf{\Theta} \tag{A4}$$

$$\mathbf{U} = \mathbf{P}_m \otimes \mathbf{C}_n,\ \mathbf{V} = \mathbf{P}_m \otimes \mathbf{S}_n,\ \mathbf{W} = \mathbf{P}_m \otimes \mathbf{C}_n,\ \mathbf{\Phi} = \mathbf{P}_m \otimes \mathbf{C}_n,\ \mathbf{\Theta} = \mathbf{P}_m \otimes \mathbf{S}_n \tag{A5}$$

$$\mathbf{P}_m = [P_0^{(\alpha,\beta)}(\phi), P_1^{(\alpha,\beta)}(\phi), \cdots, P_m^{(\alpha,\beta)}(\phi), \cdots, P_M^{(\alpha,\beta)}(\phi)] \tag{A6}$$

$$\mathbf{C}_n = [\cos(0\theta), \cos(1\theta), \cdots \cos(n\theta), \cdots, \cos(N\theta)] \tag{A7}$$

$$\mathbf{S}_n = [\sin(0\theta), \sin(1\theta), \cdots \sin(n\theta), \cdots, \sin(N\theta)] \tag{A8}$$

$$\mathbf{K} = \mathbf{K}_\xi + \mathbf{K}_b + \mathbf{K}_s \tag{A9}$$

$$\mathbf{K}_\xi = diag\left[\mathbf{K}_\xi^1, \mathbf{K}_\xi^2, \cdots, \mathbf{K}_\xi^H\right] \tag{A10}$$

$$\mathbf{K}_\xi^i = \int_{\varphi_{\xi,i}}^{\varphi_{\xi,i+1}} \int_0^{2\pi} \begin{bmatrix} K_{\xi,uu} & K_{\xi,uv} & K_{\xi,uw} & K_{\xi,u\varphi} & K_{\xi,u\theta} \\ K_{\xi,uv}^T & K_{\xi,vv} & K_{\xi,vw} & K_{\xi,v\varphi} & K_{\xi,v\theta} \\ K_{\xi,uw}^T & K_{\xi,vw}^T & K_{\xi,ww} & K_{\xi,w\varphi} & K_{\xi,w\theta} \\ K_{\xi,u\varphi}^T & K_{\xi,v\varphi}^T & K_{\xi,w\varphi}^T & K_{\xi,\varphi\varphi} & K_{\xi,\varphi\theta} \\ K_{\xi,u\theta}^T & K_{\xi,v\theta}^T & K_{\xi,w\theta}^T & K_{\xi,\varphi\theta}^T & K_{\xi,\theta\theta} \end{bmatrix} ABd\varphi d\theta \tag{A11}$$

$$\mathbf{K}_b = diag[\mathbf{K}_{bl}, 0, \cdots, \mathbf{K}_{br}] \tag{A12}$$

$$\mathbf{K}_{bl} = \int_0^{2\pi} diag\left[\mathbf{K}_{bl,uu}, K_{bl,vv}, K_{bl,ww}, K_{bl,\varphi\varphi}, K_{bl,\theta\theta}\right]_{\varphi=\varphi_0} Bd\theta \tag{A13}$$

$$\mathbf{K}_{br} = \int_0^{2\pi} diag\left[K_{br,uu}, K_{br,vv}, K_{br,ww}, K_{br,\varphi\varphi}, K_{br,\theta\theta}\right]_{\varphi=\varphi_1} Bd\theta \tag{A14}$$

$$\mathbf{K}_s = diag\left[\mathbf{K}_s^1, \mathbf{K}_s^2, \cdots, \mathbf{K}_s^H\right] \tag{A15}$$

$$\mathbf{K}_s^i = \int_0^{2\pi} \begin{bmatrix} K_{s0} & K_{s1} \\ K_{s1}^T & K_{s2} \end{bmatrix} Bd\theta \tag{A16}$$

$$\mathbf{K}_{s0} = diag\left[\mathbf{K}_{u_iu_i}, \mathbf{K}_{v_iv_i}, \mathbf{K}_{w_iw_i}, \mathbf{K}_{\varphi_i\varphi_i}, \mathbf{K}_{\varphi_i\varphi_i}\right] \tag{A17}$$

$$\mathbf{K}_{s1} = diag\left[\mathbf{K}_{u_iu_{i+1}}, \mathbf{K}_{v_iv_{i+1}}, \mathbf{K}_{w_iw_{i+1}}, \mathbf{K}_{\varphi_i\varphi_{i+1}}, \mathbf{K}_{\varphi_i\varphi_{i+1}}\right] \tag{A18}$$

$$\mathbf{K}_{s2} = diag\left[\mathbf{K}_{u_{i+1}u_{i+1}}, \mathbf{K}_{v_{i+1}v_{i+1}}, \mathbf{K}_{w_{i+1}w_{i+1}}, \mathbf{K}_{\varphi_{i+1}\varphi_{i+1}}, \mathbf{K}_{\varphi_{i+1}\varphi_{i+1}}\right] \tag{A19}$$

$$U_S^i = \frac{1}{2}\iiint \left\{ \begin{array}{l} A_{11}\left(\frac{1}{A}\frac{\partial u^i}{\partial \varphi} + \frac{v^i}{AB}\frac{\partial A}{\partial \theta} + \frac{w^i}{R_\varphi}\right)^2 + A_{22}\left(\frac{1}{B}\frac{\partial v^i}{\partial \theta} + \frac{u^i}{AB}\frac{\partial B}{\partial \varphi} + \frac{w^i}{R_\theta}\right)^2 \\ +A_{66}\left(\frac{A}{B}\frac{\partial}{\partial \theta}\left(\frac{u^i}{A}\right) + \frac{B}{A}\frac{\partial}{\partial \varphi}\left(\frac{v^i}{B}\right)\right)^2 + \\ 2A_{12}\left(\frac{1}{A}\frac{\partial u^i}{\partial \varphi} + \frac{v^i}{AB}\frac{\partial A}{\partial \theta} + \frac{w^i}{R_\varphi}\right)\left(\frac{1}{B}\frac{\partial v^i}{\partial \theta} + \frac{u^i}{AB}\frac{\partial B}{\partial \varphi} + \frac{w^i}{R_\theta}\right) + \\ +\overline{\kappa}A_{66}\left(\frac{1}{A}\frac{\partial w^i}{\partial \varphi} - \frac{u^i}{R_\varphi} + \psi_\varphi^i\right)^2 + \overline{\kappa}A_{66}\left(\frac{1}{B}\frac{\partial w^i}{\partial \theta} - \frac{v^i}{R_\theta} + \psi_\theta^i\right)^2 \end{array} \right\} AB d\varphi d\theta dz \quad \text{(A20)}$$

$$U_B^i = \frac{1}{2}\iiint \left\{ \begin{array}{l} D_{11}\left(\frac{1}{A}\frac{\partial \psi_\varphi^i}{\partial \varphi} + \frac{\psi_\theta^i}{AB}\frac{\partial A}{\partial \theta}\right)^2 + D_{22}\left(\frac{1}{B}\frac{\partial \psi_\theta^i}{\partial \theta} + \frac{\psi_\varphi^i}{AB}\frac{\partial B}{\partial \varphi}\right)^2 \\ +D_{66}\left(\frac{A}{B}\frac{\partial}{\partial \theta}\left(\frac{\psi_\varphi^i}{A}\right) + \frac{B}{A}\frac{\partial}{\partial \varphi}\left(\frac{\psi_\theta^i}{B}\right)\right)^2 \\ +2D_{12}\left(\frac{1}{A}\frac{\partial \psi_\varphi^i}{\partial \varphi} + \frac{\psi_\theta^i}{AB}\frac{\partial A}{\partial \theta}\right)\left(\frac{1}{B}\frac{\partial \psi_\theta^i}{\partial \theta} + \frac{\psi_\varphi^i}{AB}\frac{\partial B}{\partial \varphi}\right) \end{array} \right\} AB d\varphi d\theta dz \quad \text{(A21)}$$

$$U_{BS}^i = \iiint \left\{ \begin{array}{l} B_{11}\left(\frac{1}{A}\frac{\partial u^i}{\partial \varphi} + \frac{v^i}{AB}\frac{\partial A}{\partial \theta} + \frac{w^i}{R_\varphi}\right)\left(\frac{1}{A}\frac{\partial \psi_\varphi^i}{\partial \varphi} + \frac{\psi_\theta^i}{AB}\frac{\partial A}{\partial \theta}\right) \\ +B_{12}\left(\frac{1}{A}\frac{\partial u^i}{\partial \varphi} + \frac{v^i}{AB}\frac{\partial A}{\partial \theta} + \frac{w^i}{R_\varphi}\right)\left(\frac{1}{B}\frac{\partial \psi_\theta^i}{\partial \theta} + \frac{\psi_\varphi^i}{AB}\frac{\partial B}{\partial \varphi}\right) \\ +B_{12}\left(\frac{1}{B}\frac{\partial v^i}{\partial \theta} + \frac{u^i}{AB}\frac{\partial B}{\partial \varphi} + \frac{w^i}{R_\theta}\right)\left(\frac{1}{A}\frac{\partial \psi_\varphi^i}{\partial \varphi} + \frac{\psi_\theta^i}{AB}\frac{\partial A}{\partial \theta}\right) + \\ B_{66}\left(\frac{1}{A}\frac{\partial u^i}{\partial \varphi} + \frac{v^i}{AB}\frac{\partial A}{\partial \theta} + \frac{w^i}{R_\varphi}\right)\left(\frac{A}{B}\frac{\partial}{\partial \theta}\left(\frac{\psi_\varphi^i}{A}\right) + \frac{B}{A}\frac{\partial}{\partial \varphi}\left(\frac{\psi_\theta^i}{B}\right)\right) \\ +B_{22}\left(\frac{1}{B}\frac{\partial v^i}{\partial \theta} + \frac{u^i}{AB}\frac{\partial B}{\partial \varphi} + \frac{w^i}{R_\theta}\right)\left(\frac{1}{B}\frac{\partial \psi_\theta^i}{\partial \theta} + \frac{\psi_\varphi^i}{AB}\frac{\partial B}{\partial \varphi}\right) \end{array} \right\} AB d\varphi d\theta dz \quad \text{(A22)}$$

References

1. Fantuzzi, N.; Brischetto, S.; Tornabene, F.; Viola, E. 2D and 3D shell models for the free vibration investigation of functionally graded cylindrical and spherical panels. *Compos. Struct.* **2016**, *154*, 573–590. [CrossRef]
2. Tornabene, F.; Reddy, J.N. FGM and Laminated Doubly-Curved and Degenerate Shells Resting on Nonlinear Elastic Foundations: A GDQ Solution for Static Analysis with a Posteriori Stress and Strain Recovery. *J. Indian Inst. Sci.* **2013**, *93*, 635–688.
3. Pradyumna, S.; Bandyopadhyay, J.N. Free vibration analysis of functionally graded curved panels using a higher-order finite element formulation. *J. Sound Vib.* **2008**, *318*, 176–192. [CrossRef]
4. Jouneghani, F.Z.; Dimitri, R.; Bacciocchi, M.; Tornabene, F. Free Vibration Analysis of Functionally Graded Porous Doubly-Curved Shells Based on the First-Order Shear Deformation Theory. *Appl. Sci.* **2017**, *7*, 1252. [CrossRef]
5. Chen, H.Y.; Wang, A.W.; Hao, Y.X.; Zhang, W. Free vibration of FGM sandwich doubly-curved shallow shell based on a new shear deformation theory with stretching effects. *Compos. Struct.* **2017**, *179*, 50–60. [CrossRef]
6. Wang, Q.S.; Cui, X.H.; Qin, B.; Liang, Q.; Tang, J.Y. A semi-analytical method for vibration analysis of functionally graded (FG) sandwich doubly-curved panels and shells of revolution. *Int. J. Mech. Sci.* **2017**, *134*, 479–499. [CrossRef]
7. Wang, Q.S.; Qin, B.; Shi, D.Y.; Liang, Q. A semi-analytical method for vibration analysis of functionally graded carbon nanotube reinforced composite doubly-curved panels and shells of revolution. *Compos. Struct.* **2017**, *174*, 87–109. [CrossRef]
8. Wang, Q.S.; Cui, X.H.; Qin, B.; Liang, Q. Vibration analysis of the functionally graded carbon nanotube reinforced composite shallow shells with arbitrary boundary conditions. *Compos. Struct.* **2017**, *182*, 364–379. [CrossRef]
9. Wang, Q.S.; Shi, D.Y.; Liang, Q.; Pang, F.Z. Free vibration of moderately thick functionally graded parabolic and circular panels and shells of revolution with general boundary conditions. *Eng. Comput.* **2017**, *34*, 1598–1641. [CrossRef]
10. Tornabene, F.; Viola, E. Free vibrations of four-parameter functionally graded parabolic panels and shells of revolution. *Eur. J. Mech. A Solids* **2009**, *28*, 991–1013. [CrossRef]
11. Viola, E.; Tornabene, F. Free vibrations of three parameter functionally graded parabolic panels of revolution. *Mech. Res. Commun.* **2009**, *36*, 587–594. [CrossRef]

12. Tornabene, F.; Viola, E. Static analysis of functionally graded doubly-curved shells and panels of revolution. *Meccanica* **2013**, *48*, 901–930. [CrossRef]
13. Fazzolari, F.A.; Carrera, E. Refined hierarchical kinematics quasi-3D Ritz models for free vibration analysis of doubly curved FGM shells and sandwich shells with FGM core. *J. Sound Vib.* **2014**, *333*, 1485–1508. [CrossRef]
14. Kar, V.R.; Panda, S.K. Free vibration responses of functionally graded spherical shell panels using finite element method. In Proceedings of the ASME 2013 Gas Turbine India Conference, Bangalore, India, 5–6 December 2013; p. V001T005A014.
15. Tornabene, F. Free vibration analysis of functionally graded conical, cylindrical shell and annular plate structures with a four-parameter power-law distribution. *Comput. Methods Appl. Mech. Eng.* **2009**, *198*, 2911–2935. [CrossRef]
16. Zghal, S.; Frikha, A.; Dammak, F. Free vibration analysis of carbon nanotube-reinforced functionally graded composite shell structures. *Appl. Math. Model.* **2018**, *53*, 132–155. [CrossRef]
17. Kulikov, G.M.; Plotnikova, S.V.; Kulikov, M.G.; Monastyrev, P.V. Three-dimensional vibration analysis of layered and functionally graded plates through sampling surfaces formulation. *Compos. Struct.* **2016**, *152*, 349–361. [CrossRef]
18. Kapuria, S.; Patni, M.; Yasin, M.Y. A quadrilateral shallow shell element based on the third-order theory for functionally graded plates and shells and the inaccuracy of rule of mixtures. *Eur. J. Mech. A Solids* **2015**, *49*, 268–282. [CrossRef]
19. Hosseini-Hashemi, S.; Derakhshani, M.; Fadaee, M. An accurate mathematical study on the free vibration of stepped thickness circular/annular Mindlin functionally graded plates. *Appl. Math. Model.* **2013**, *37*, 4147–4164. [CrossRef]
20. Bambill, D.V.; Rossit, C.A.; Felix, D.H. Free vibrations of stepped axially functionally graded Timoshenko beams. *Meccanica* **2015**, *50*, 1073–1087. [CrossRef]
21. Vinyas, M.; Kattimani, S.C. Static analysis of stepped functionally graded magneto-electro-elastic plates in thermal environment: A finite element study. *Compos. Struct.* **2017**, *178*, 63–86. [CrossRef]
22. Vinyas, M.; Kattimani, S.C. Static studies of stepped functionally graded magneto-electro-elastic beam subjected to different thermal loads. *Compos. Struct.* **2017**, *163*, 216–237. [CrossRef]
23. Su, Z.; Jin, G.Y.; Ye, T.G. Vibration analysis of multiple-stepped functionally graded beams with general boundary conditions. *Compos. Struct.* **2018**, *186*, 315–323. [CrossRef]
24. Li, H.; Pang, F.; Chen, H.; Du, Y. Vibration analysis of functionally graded porous cylindrical shell with arbitrary boundary restraints by using a semi analytical method. *Compos. Part B Eng.* **2019**, *164*, 249–264. [CrossRef]
25. Li, H.; Pang, F.; Wang, X.; Du, Y.; Chen, H. Free vibration analysis for composite laminated doubly-curved shells of revolution by a semi analytical method. *Compos. Struct.* **2018**, *201*, 86–111. [CrossRef]
26. Tornabene, F.; Fantuzzi, N.; Bacciocchi, M.; Reddy, J.N. An Equivalent Layer-Wise Approach for the Free Vibration Analysis of Thick and Thin Laminated and Sandwich Shells. *Appl. Sci.* **2017**, *7*, 17. [CrossRef]
27. Tornabene, F.; Fantuzzi, N.; Bacciocchi, M. A new doubly-curved shell element for the free vibrations of arbitrarily shaped laminated structures based on Weak Formulation IsoGeometric Analysis. *Compos. Struct.* **2017**, *171*, 429–461. [CrossRef]
28. Tornabene, F.; Fantuzzi, N.; Bacciocchi, M.; Viola, E. Effect of agglomeration on the natural frequencies of functionally graded carbon nanotube-reinforced laminated composite doubly-curved shells. *Compos. Part B Eng.* **2016**, *89*, 187–218. [CrossRef]
29. Tornabene, F.; Fantuzzi, N.; Viola, E.; Batra, R.C. Stress and strain recovery for functionally graded free-form and doubly-curved sandwich shells using higher-order equivalent single layer theory. *Compos. Struct.* **2015**, *119*, 67–89. [CrossRef]
30. Li, H.; Pang, F.; Wang, X.; Li, S. Benchmark Solution for Free Vibration of Moderately Thick Functionally Graded Sandwich Sector Plates on Two-Parameter Elastic Foundation with General Boundary Conditions. *Shock Vib.* **2017**, *2017*, 4018629. [CrossRef]
31. Li, H.; Liu, N.; Pang, F.; Du, Y.; Li, S. An Accurate Solution Method for the Static and Vibration Analysis of Functionally Graded Reissner-Mindlin Rectangular Plate with General Boundary Conditions. *Shock Vib.* **2018**, *2018*, 4535871. [CrossRef]

32. Zhong, R.; Wang, Q.; Tang, J.; Shuai, C.; Qin, B. Vibration analysis of functionally graded carbon nanotube reinforced composites (FG-CNTRC) circular, annular and sector plates. *Compos. Struct.* **2018**, *194*, 49–67. [CrossRef]
33. Fantuzzi, N.; Tornabene, F.; Viola, E. Four-parameter functionally graded cracked plates of arbitrary shape: A GDQFEM solution for free vibrations. *Mech. Adv. Mater. Struct.* **2016**, *23*, 89–107. [CrossRef]
34. Choe, K.; Tang, J.; Shui, C.; Wang, A.; Wang, Q. Free vibration analysis of coupled functionally graded (FG) doubly-curved revolution shell structures with general boundary conditions. *Compos. Struct.* **2018**, *194*, 413–432. [CrossRef]
35. Zhao, J.; Zhang, Y.; Choe, K.; Qu, X.; Wang, A.; Wang, Q. Three-dimensional exact solution for the free vibration of thick functionally graded annular sector plates with arbitrary boundary conditions. *Compos. Part B Eng.* **2019**, *159*, 418–436. [CrossRef]
36. Zhao, J.; Choe, K.; Xie, F.; Wang, A.; Shuai, C.; Wang, Q. Three-dimensional exact solution for vibration analysis of thick functionally graded porous (FGP) rectangular plates with arbitrary boundary conditions. *Compos. Part B Eng.* **2018**, *155*, 369–381. [CrossRef]
37. Guo, J.; Shi, D.; Wang, Q.; Tang, J.; Shuai, C. Dynamic analysis of laminated doubly-curved shells with general boundary conditions by means of a domain decomposition method. *Int. J. Mech. Sci.* **2018**, *138–139*, 159–186. [CrossRef]
38. Pang, F.; Li, H.; Du, Y.; Li, S.; Chen, H.; Liu, N. A Series Solution for the Vibration of Mindlin Rectangular Plates with Elastic Point Supports around the Edges. *Shock Vib.* **2018**, *2018*, 8562079. [CrossRef]
39. Li, H.; Pang, F.; Chen, H. A semi-analytical approach to analyze vibration characteristics of uniform and stepped annular-spherical shells with general boundary conditions. *Eur. J. Mech. A Solids* **2019**, *74*, 48–65. [CrossRef]
40. Li, H.; Pang, F.; Miao, X.; Du, Y.; Tian, H. A semi-analytical method for vibration analysis of stepped doubly-curved shells of revolution with arbitrary boundary conditions. *Thin-Walled Struct.* **2018**, *129*, 125–144. [CrossRef]
41. Li, H.; Pang, F.; Miao, X.; Li, Y. Jacobi–Ritz method for free vibration analysis of uniform and stepped circular cylindrical shells with arbitrary boundary conditions: A unified formulation. *Comput. Math. Appl.* **2018**. [CrossRef]
42. Li, H.; Pang, F.; Wang, X.; Du, Y.; Chen, H. Free vibration analysis of uniform and stepped combined paraboloidal, cylindrical and spherical shells with arbitrary boundary conditions. *Int. J. Mech. Sci.* **2018**, *145*, 64–82. [CrossRef]
43. Pang, F.; Li, H.; Wang, X.; Miao, X.; Li, S. A semi analytical method for the free vibration of doubly-curved shells of revolution. *Comput. Math. Appl.* **2018**, *75*, 3249–3268. [CrossRef]
44. Bhrawy, A.H.; Taha, T.M.; Machado, J.A.T. A review of operational matrices and spectral techniques for fractional calculus. *Nonlinear Dyn.* **2015**, *81*, 1023–1052. [CrossRef]
45. Pang, F.; Li, H.; Choe, K.; Shi, D.; Kim, K. Free and Forced Vibration Analysis of Airtight Cylindrical Vessels with Doubly Curved Shells of Revolution by Using Jacobi-Ritz Method. *Shock Vib.* **2017**, *2017*, 4538540. [CrossRef]
46. Qu, Y.; Long, X.; Yuan, G.; Meng, G. A unified formulation for vibration analysis of functionally graded shells of revolution with arbitrary boundary conditions. *Compos. Part B Eng.* **2013**, *50*, 381–402. [CrossRef]
47. Martínez-Pañeda, E.; Gallego, R. Numerical analysis of quasi-static fracture in functionally graded materials. *Int. J. Mech. Mater. Des.* **2015**, *11*, 405–424. [CrossRef]